CSMA 2017
13ème Colloque National en Calcul des Structures
15-19 Mai 2017, Presqu'île de Giens (Var)

Non-linear dynamics in torsional micromirrors

A. Frangi[1], A. Guerrieri, N. Boni

[1] *Department of Civil and Environmental Engng., Politecnico di Milano, Milano, 20133 Italy, attilio.frangi@polimi.it*

Abstract — The main torsional mode of electrostatically in-plane actuated micromirrors is known to be driven by parametric resonance. Here we show that also a spurious yaw mode is activated by the same phenomenon and it eventually interacts with the main torsional response. Furthermore, we experimentally observe that the coupling between the two modes is higly sensitive to temperature variations and we finally present a numerical model capable to capture the key phenomena.
Keywords — Micromirrors, MOEMS, Parametric resonance, Mathieu equation, Continuation techniques, Large displacements, Temperature effect.

1 Introduction

Micromirros are one of the key components within the family of Optical Micro-Electro-Mechanical-Systems (MOEMS). They are diffused in many applications such as pico-projectors for compact portable devices and micro-scanner for real-time 3D shape measurement of moving objects (see [1, 2, 3]). Nowadays we can find several designs characterized by different driving principles (magnetic, thermal, piezoelectric and electrostatic). This work analyses the non-linear response of a torsional micromirror (depicted in Figure 1) electrostatically actuated by means of comb-finger capacitors and a square wave voltage input. It is well known [10, 8, 14, 13, 5, 4] that electrostatic actuation excites the main torsional mode by parametric resonance (and not by standard harmonic one) and it has a softening effect on it. Here we additionally show that parametric resonance, together with geometrical nonlinearities arising from large rotations, activates also a spurious hardening yaw mode affecting the close-to-peak frequency of the torsional motion. Furthermore, the spurious mode, being highly sensitive to temperature, can be easily shifted in or out the frequency ranges of the main one.

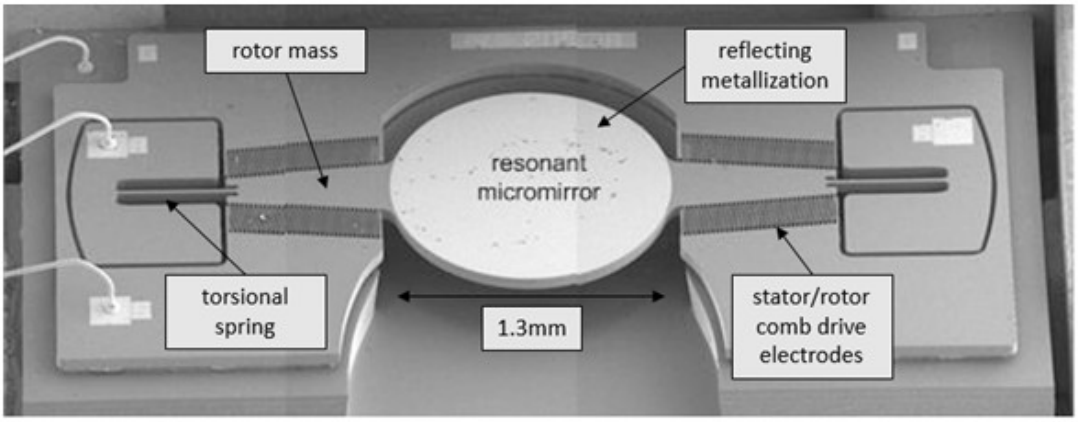

Figure 1: SEM image of the micromirror device

2 Micromirror device

The device has been fabricated with a dedicated SOI technology. The central circular reflecting surface is attached to the substrate via two coaxial beams. Four sets of 33 fingers each are anchored to the trapezoidal regions directly attached to the mirror. These plates, interdigited with their stator counterparts,

form a comb drive structure providing the electrostatic actuation mechanism. Sensing of the opening angle is performed, during operation, via the same comb drive electrodes.

2.1 Equations of motion

In the simulations the mirror is treated as a rigid body hinged in its centre so that the three Euler angles (roll ψ, pitch ϕ and yaw θ) completely define its configuration. In the main mode the mirror rolls around the axis of the springs while, in the spurious one, it yaws in its plane around an axis passing through its centre. The equation of motion for the rigid mirror are written in the moving frame attached to the rotating mass and with origin its centre:

$$I_\phi \dot{\omega}_\phi + I_\phi B_\phi \omega_\phi + (I_\psi - I_\theta)\omega_\theta \omega_\psi = M_\phi(\psi, \theta, \phi) \tag{1}$$

$$I_\theta \dot{\omega}_\theta + I_\theta B_\theta \omega_\theta + (I_\phi - I_\psi)\omega_\phi \omega_\psi = M_\theta(\psi, \theta, \phi) \tag{2}$$

$$I_\psi \dot{\omega}_\psi + I_\psi B_\psi \omega_\psi + (I_\theta - I_\phi)\omega_\phi \omega_\theta = M_\psi(\psi, \theta, \phi) \tag{3}$$

where I_i are the principal moment of inertia in the moving frame. The couples $M_i = M_{i,c} + M_{i,e}$ account for both elastic restoring actions and electrostatic actuation. The electrostatic contribution is obtained as described in Section 2.2 while the mechanical actions are computed using a FEM code for beams in large transformations, as detailed in Section 2.3. The challenging estimation of gas damping coefficients is solved in a naive but effective way. A constant B_ψ parameter is tuned to fit the experimental quality factor of the main mode. An incompressible Stokes solver (see [7]) is used to estimate B_θ for the small-amplitude yaw mode.

2.2 Electrostatic actuation

The mirror is excited near the resonance peak (close to 5.3kHz) and the phase between the driving signal and the mirror is kept constant by a closed loop. The mirror is driven with a "trapezoidal" wave at 150V and a typical duration <25% of the duty cycle. The FFT of the input signal shows that the 2:1 parametric resonance can activate the spurious yaw mode, its resonance frequency being around 18kHz.

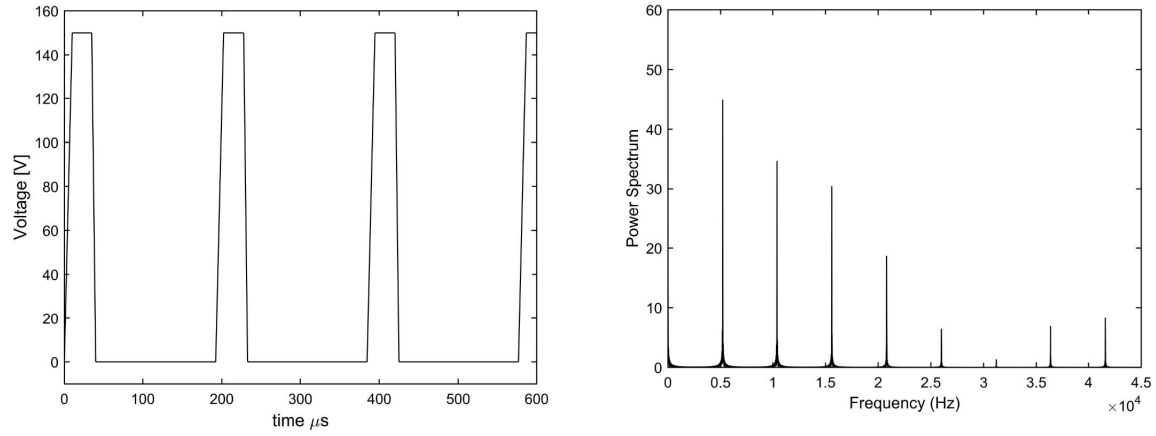

Figure 2: Driving input signal at 5.3kHz. Representation in time and frequency spaces

$$M_{i,c} = \frac{1}{2}\varepsilon_0 V(t)^2 [S]^T \begin{pmatrix} 0 \\ C_{g,\theta} \\ C_{g,\psi} \end{pmatrix} \tag{4}$$

Here $\varepsilon_0 = 8.85 \times 10^{-6} pF/\mu$m is the void dielectric constant, V in volts is the driving input signal, $[S]$ is a transformation matrix that allow to transform Euler angles variations into angular variations in the moving frame attached to the mirror; finally $C_{g,i}$ (in microns) denotes the geometric capacitance variation with respect to the i-th angle.

The capacitance is computed numerically by means of a dedicated code based on integral equations and is assumed to be a function of both the torsional ψ and yaw θ angles of the rigid mirror. Next we use second order accurate numerical differentiation in order to compute capacitance variations.

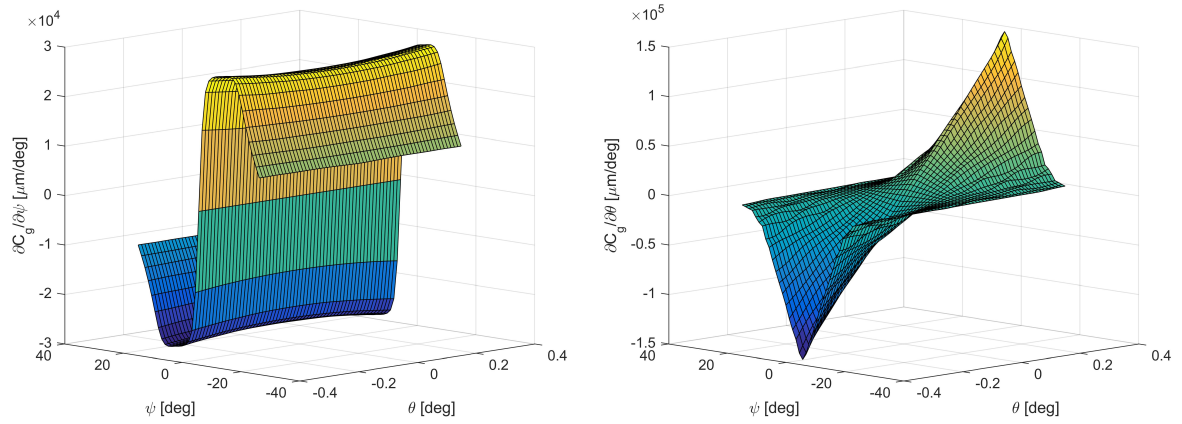

Figure 3: Geometrical capacitance derivatives with respect ψ torsional and θ yaw angle

2.3 Elastic restoring forces

A general formulation for beams in large transformations (see [11, 12]) has been implemented in a FEM code. This captures both the geometrical nonlinear effects of large rotations and the coupling between roll, pitch and yaw modes. Each of the two torsional springs is modeled as a cantilever beam (clamped on one side) subjected on the free side to imposed displacements and rotations following the rigid body rotation of the mirror. Assuming rigid cross sections, the actual configuration $\{x\}$ of the beam is completely defined by the displacement of the cross section center $\{u\}$ and its rotation tensor $[\Lambda]$ through the Euler-Rodriguez formula for exponential mapping. Let $X_3\{e_3\}$ be the position vector of points along the beam axis in the original configuration:

$$\{x\} = \{X_0(X_3)\} + \{u(X_3)\} + \sum_{\alpha=1}^{2} X_\alpha [\Lambda(X_3)]\{e_\alpha(X_3)\} \tag{5}$$

$$[\Lambda(X_3)] = \mathrm{diag}(1,1,1) + \sin\varphi[k_\wedge] + (1+\cos\varphi)[k_\wedge][k_\wedge] = e^{[\varphi_\wedge]} \tag{6}$$

With the notation $[\varphi_\wedge] = \varphi[k_\wedge]$ we define the skew symmetric tensor of the Euler-Rodriguez axial vector $\{\varphi\}$ with modulus φ. We assume that the mass of the torsional springs is negligible with respect to that of the mirror. The equations governing the static equilibrium of beams in large transformations are written in the rotated reference frame:

$$R(\{u\},\{\varphi\};\{\tilde{u}\},\{\tilde{\varphi}\}) = \int_0^L [\{n\}^T(\{\tilde{u}'\} + [x'_{0\wedge}]\{\tilde{\varphi}'\}) + \{m\}^T\{\tilde{\varphi}'\}]ds \tag{7}$$

where the prime denotes differentiation wrt X_3. Generalized sectional stress resultants $\{n\}$ and $\{m\}$ depend non linearly on the unknown kinematic fields, i.e. displacements $\{u\}$ and rotations $\{\varphi\}$. Assuming small strains, the backrotated stress resultants $\{N\}$ and $\{M\}$ are linear functions of material strains $\{\Gamma\}$ (plus the thermal contribution) and curvatures $\{K\}$:

$$\{N\} = [\Lambda]^T\{n\} = [C_N](\{\Gamma\} - \alpha\Delta T\{e_3\}) \tag{8}$$

$$\{M\} = [\Lambda]^T\{m\} = [C_M]\{K\} \tag{9}$$

and:

$$\{C_N\} = \mathrm{diag}(GA^*, GA^*, EA) = [\Lambda]^T [c_N][\Lambda] \tag{10}$$

$$\{C_M\} = \mathrm{diag}(EJ_{11}, EJ_{22}, GJ_t) = [\Lambda]^T [c_M][\Lambda] \tag{11}$$

$$\{\Gamma\} = [\Lambda]^T (\{u'\} + \{e_3\}) - \{e_3\} \tag{12}$$

$$\{K\} = [T]^T \{\varphi'\} \tag{13}$$

$$[T] = \mathrm{diag}(1,1,1) + \frac{(1+\cos\varphi)}{\varphi}[k_\wedge] + \frac{(\varphi - \sin\varphi)}{\varphi}[k_\wedge][k_\wedge] \tag{14}$$

Finally a Newton-Ralphson scheme is adopted to solve the nonlinear variational system of equations.

3 Experimental and numerical results

The monitoring of the opening angle of the electrostatic micro-mirror was obtained through the experimental measurement of the deflection of a laser beam incident on the device. The resonant movement of the mirror projects on a target a laser segment which is acquired by a camera and then processed. The control software gives the possibility to set the scanning frequency range, step and direction of sweep (up or down).

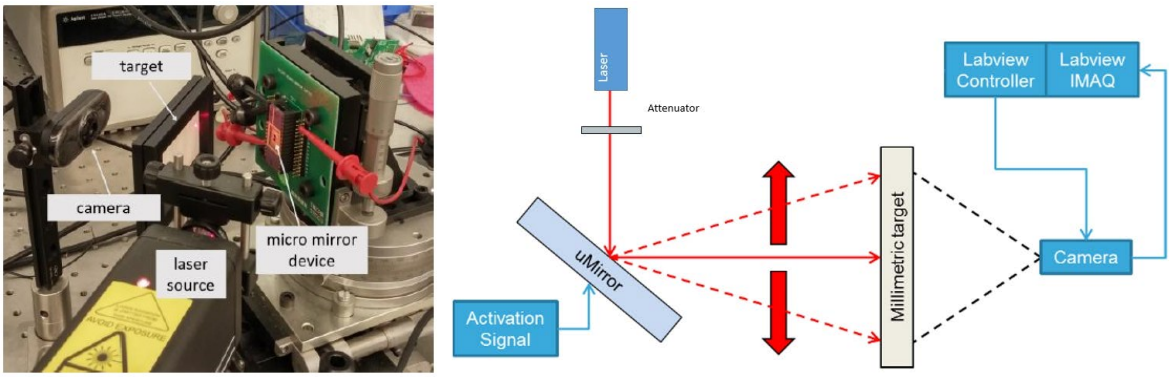

Figure 4: Setup used for the characterization of the mirror

The numerical simulation ha been performed both with a “brute force” approach, and with a more refined “continuation” technique [6].

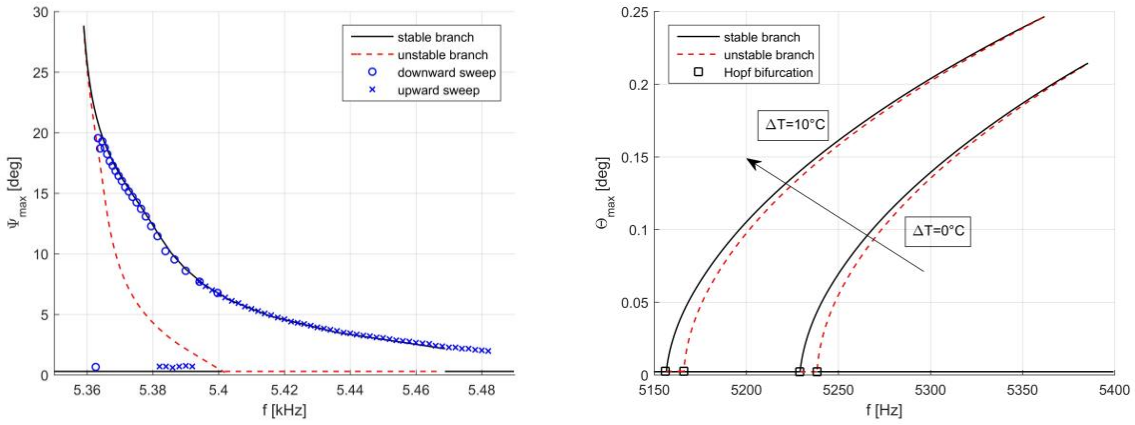

(a) (b)

Figure 5: Uncoupled modes. (a) Main torsional softening mode. Experimental data (circles and crosses) and numerical simulation (continuous and dashed lines); (b) Simulation of the spurious hardening yaw mode alone ($\psi = 0$)

In the former case amplitude vs. frequency plots are obtained by direct analysis in time. A sweep over the frequencies of interest is performed and for each frequency a sufficient number of cycles are simulated by direct integration to reach a steady state; the amplitude is then recorded and the next frequency is addressed, using the final amplitude and phase of the previous analysis as initial conditions. This is a very robust technique which however permits to simulate only the stable branches of the response. On the contrary, the continuation approach with arc length control is more accurate and general. To this purpose a custom numerical code has been implemented to simulate single mode responses while AUTO software [6] has been used for the analysis of the complete coupled problem.

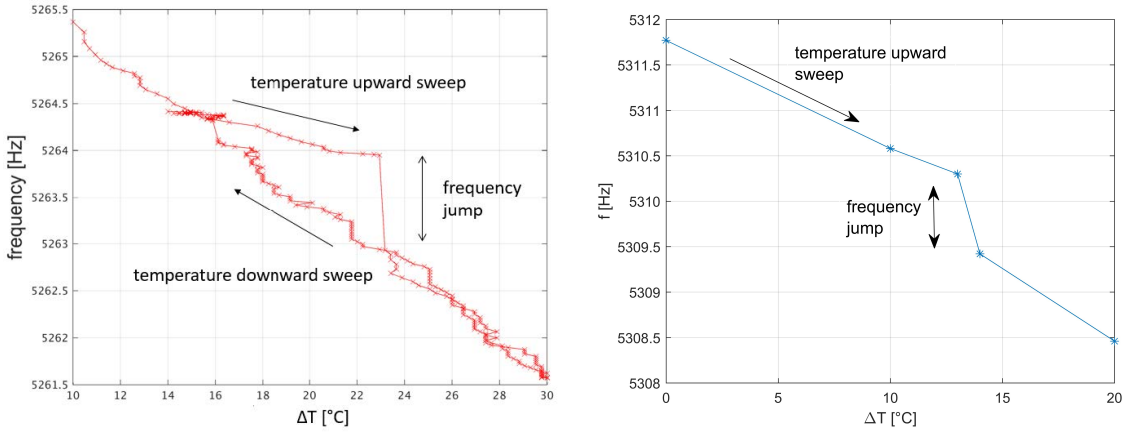

(a) (b)

Figure 6: Coupled modes. (a) Frequency of the torsional mode (phase control) close-to-peak. Sensitivity to ambient temperature (experimental data); (b) Frequency of the torsional mode (phase control) close-to-peak. Sensitivity to ambient temperature (AUTO simulation); upward sweep

Increasing the frequency of the input square wave, the mirror's motion is activated whenever there exists an integer n such that $n\omega = 2\omega_0$. For instance, for $\omega \simeq 5kHz$ we have $n = 2$ for the main mode and $n = 7$ for the spurious one. It is worth stressing that the development of the ad-hoc code has been stimulated specifically to avoid an approximate representation of the square wave as finite sum of sinusoidal components inducing spurious Gibbs oscillations.

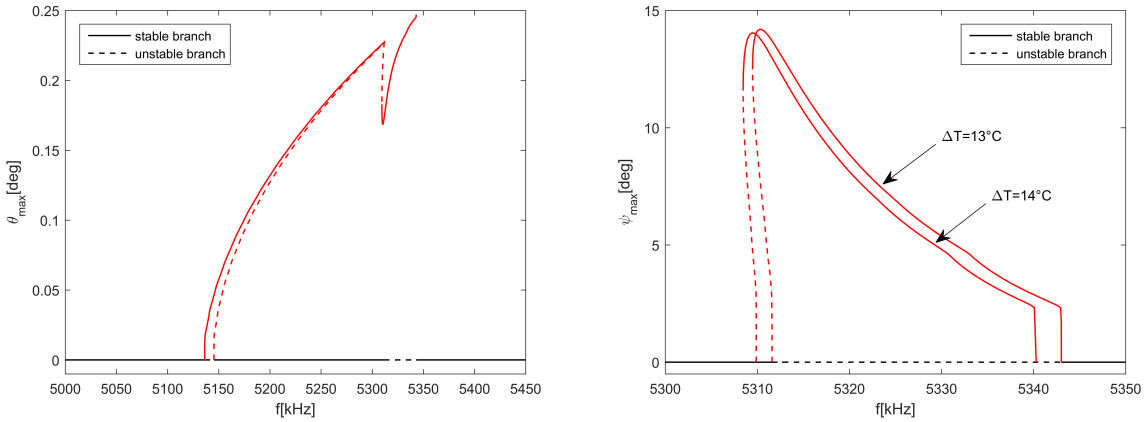

(a) (b)

Figure 7: Coupled modes. (a) Spurious hardening yaw mode (AUTO). Before frequency jump; (b) Main torsional softening mode (AUTO).Before and after frequency jump.

Figure 6 plots the frequency (in phase control) of the torsional mode as the temperature is varied. Increasing the temperature, at a critical level of T the frequency drops of about 1Hz. This occurs because the modes are coupled and the spurious one is eventually shifted to the left of the main mode frequency range. Numerical simulations obtained with both approaches predict a quantitatively correct frequency

jump. The Young modulus is considered temperature dependent in the simulations with a variation of -60ppm/°C. The phenomenon can be understood if we look at the response curves of Figure 7. When the temperature is lower than the critical one, the spurious mode falls in the frequency range of the main torsional mode. This is reflected in the V-shaped response curve of the yaw mode induced by the interaction with the torsional motion. As the temperature is increased beyond the critical level, the frequency domains of the two modes become completely decoupled and main mode shitfs towards lower frequencies and lower amplitudes.

4 Conclusions

In this paper we have analysed the dynamic response of an electrotatically actuated micromirror. The results obtained with a numerical model are investigate and validated against laboratory tests on a real device. The experimental data are reproduced with very good accuracy. We have shown that parametric resonance is the phenomenon responsible for the motion of this kind of devices. Indeed, it excites not only the main torsional response, as it is well known, but also a spurious yaw mode. A model for beams in large transformations and a complete set of equations of motion are required to capture the mirror's modal coupling. Furthermore, we have pointed out that temperature has a key role in the dynamic response of the device. As temperature increases, the proposed numerical model is able to replicate experimental evidences showing a sudden jump in the close-to-peak torsional frequency in phase control. We have shown that this phenomenon is directly linked to the frequency drift of the yaw response curve induced by its high temperature sensitivity.

References

[1] Intel, Real Sense Technology, http://www.intel.it

[2] Micro-mirrors from STMicroelectronics Provide Precision in Perceptual Computing, http://www.st.com/web/en/press/p3657

[3] Lab4MEMS II, Micro-Optical MEMS, micro-mirros and pico-projectors, ENIAC Project, http://www.lab4mems2.ite.waw.pl/

[4] Carr D.W., Evoy S., Sekaric L., Craighead H.G., Parpia J.M., Parametric amplification in a torsional microresonator. *Applied Physics Letters*, 77, 2000

[5] A. Caspani, C. Comi, A. Corigliano, G. Langfelder, V. Zega, S. Zerbini, Dynamic nonlinear behavior of torsional resonators in MEMS, *J. Micromech. Microeng.*, 24, 095025, 2014

[6] E.J. Doedel, J.P. Kernévez, Auto: Software for continuation problems in ordinary differential equations with applications, *Applied Mathematics*, California Institute of Technology, Pasadena, 1986.

[7] Frangi A., Spinola G., Vigna B., On the evaluation of damping in MEMS in the slip-flow regime, *Int. J. Numerical Methods in Engineering*, 68, 1031–1051, 2006

[8] M.I. Younis, *MEMS Linear and Nonlinear Statics and Dynamics*, Springer, 2011

[9] R. Mirzazadeh, S. Mariani, M. De Fazio, Modeling of Fluid Damping in Resonant Micro-Mirrors with Out-of-Plane Comb-Drive Actuation, *International Electronic Conference on Sensors and Applications*, 2014

[10] Shahid W., Qiu Z., Duan X., Li H., Wang T.D., Oldham K.R., Modeling and Simulation of a Parametrically Resonant Micromirror With Duty-Cycled Excitation, *JMEMS*, vol. 23, pp. 1440-1453, 2014

[11] Simo J.C., Vu-Quoc L. A three-dimensional finite strain rod model. Part II: computational aspects, *Comp. Meth. Appl. Mech. Engng.*, 58, 79–116, 1986

[12] Simo J.C., Vu-Quoc L. On the dynamics in space of rods undergoing large motions. A geometrically exact approach, *Comp. Meth. Appl. Mech. Engng.*, 66, 125–161, 1988

[13] Taghizadeh M., Mobki H., Bifurcation analysis of torsional micromirror actuated by electrostatic forces, *Archives of Mechanics*, vol. 66, pp. 95–111, 2014

[14] Zhang X.M., Chau F.S., Quan C., Lam Y.L., Liu A.Q., A study of the static characteristics of a torsional micromirror, *Sensors and Actuators A: Physical*, vol. 90, pp. 73–81, 2001